Self-Replicating Cracks: A Collaborative Fracture Mode in Thin Films

Joël Marthelot,[1,2,*] Benoît Roman,[1] José Bico,[1] Jérémie Teisseire,[2] Davy Dalmas,[2] and Francisco Melo[3]
[1]PMMH, CNRS UMR 7636, UPMC Université Paris 6, and Université Paris Diderot Paris 7, ESPCI-ParisTech, 10 Rue Vauquelin, 75231 Paris Cedex 05, France
[2]SVI, CNRS UMR 125, Saint-Gobain Recherche, BP 135, 93303 Aubervilliers Cedex, France
[3]Departamento de Física, Universidad de Santiago de Chile, Avenida Ecuador 3493, 9170124 Estación Central, Santiago, Chile
(Received 28 May 2014; published 20 August 2014)

Straight cracks are observed in thin coatings under residual tensile stress, resulting into the classical network pattern observed in china crockery, old paintings, or dry mud. Here, we present a novel fracture mechanism where delamination and propagation occur simultaneously, leading to the spontaneous self-replication of an initial template. Surprisingly, this mechanism is active below the standard critical tensile load for channel cracks and selects a robust interaction length scale on the order of 30 times the film thickness. Depending on triggering mechanisms, crescent alleys, spirals, or long bands are generated over a wide range of experimental parameters. We describe with a simple physical model, the selection of the fracture path and provide a configuration diagram displaying the different failure modes.

DOI: 10.1103/PhysRevLett.113.085502 PACS numbers: 62.20.mm, 68.60.Bs, 81.16.Rf, 81.20.Fw

Nanometer to micrometer thin film coatings are extensively used in material science to protect and functionalize surfaces [1], from traditional thermal barriers [2], mechanical or chemical protection, to more recent applications in biomedical [3] or stretchable electronics [4]. However, deposition processes, thermal expansion mismatch, or simply mechanical loading generally result into compressive or tensile residual stresses that induce two main types of failure of coatings. Compressive stresses commonly induce the formation of wrinkles [5] and blisters [1,6] whereas tensile stresses leads to straight *channel cracks* across the film thickness [7]. Once triggered, these fractures propagate along a straight trajectory, being only deflected in the close vicinity of a previous fracture path, where they tend to connect perpendicularly to the free boundary. In the case of a stiff substrate, this interaction distance is on the order of the thickness of the coating. Such familiar hierarchical disordered patterns are, for instance, observed in dry mud [8,9], in the glaze of ceramics, or even in plant venation and urban networks [10]. Delamination may eventually occur after the previous fracture pattern has been established [11].

This scenario is observed in our experiments with thick coatings of commercial spin-on glass (SOG) trimethylsiloxane when adhesion is enhanced by a plasma treatment of the substrate. In such coatings, which are commonly used for adjusting the optical index of buffer layers in laser cavities, residual biaxial stresses result from a sol-gel process. However, unexpected crack morphologies [Fig. 1(a)] are observed in the case of moderate adhesion ($\Gamma \sim 0.5$ J/m^2). Decreasing the density of defects (e.g., by filtering the SOG solution prior to reaction) leads to intriguing patterns. Archimedean spirals [Fig. 1(b)], crescent alleys [Figs. 1(c)–1(d)], or parallel bands [Figs. 1(e)–1(f)] grow spontaneously after the sol-gel condensation reaction on a silicon wafer as the sample is removed from the reacting chamber (see movies S1, S2, and S3 in the Supplemental Material [12]). These cracks are triggered by sporadic defects in the coating but can also be induced locally by the operator (e.g., several fractures randomly initiate from the scratch of a sharp

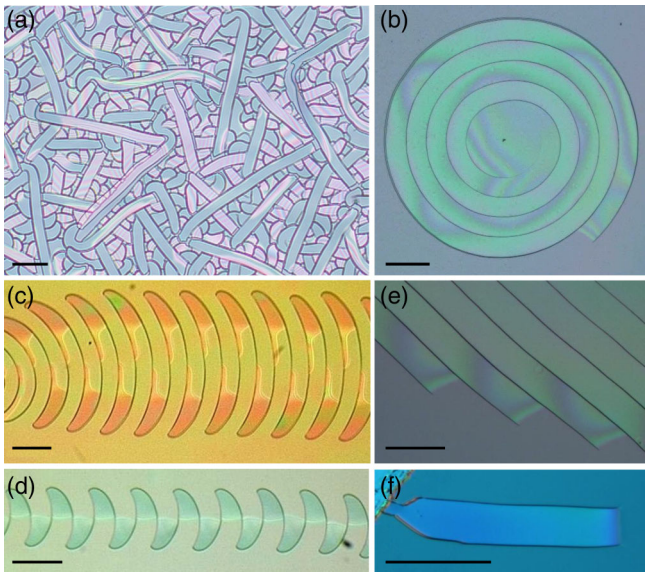

FIG. 1 (color online). Unusual cracks in thin film moderately adherent to a substrate (scale bar 100 μm). Numerous nucleation spots lead to complex patterns (a). Self-replicating cracks triggered by scarce defects (see the supporting movies S1, S2, S3 in the Supplemental Material [12]): Archimedean spirals (b); regular alleys of crescents (c),(d); and parallel bands (e) follow an initial arch, loop, or line, at a fixed distance W_1. (f) Pairs of cracks simultaneously follow each other path leading to isolated bands.

blade). As they propagate, cracks tend to follow a previous cut at a fixed distance. Crescent alleys, spirals, and series of parallel bands thus correspond to the self-replication of an initial arch, loop, or line, respectively. The growth of an isolated band can also be viewed as a pair of cracks following simultaneously each other's path.

These patterns are strikingly different from usual crazing glaze figures, but they are not specific to the SOG system studied in this Letter. Indeed, similar crescent alleys or spiral patterns have been mentioned in different areas of material science [13–20]. However, the corresponding fracture mechanism remains mysterious.

We carried experiments on SOG layers with different thicknesses and adhesion properties (deposition and characterization of the coating are described in the Supplemental Material [12]). We present in Fig. 2 the characteristic length scale of the patterns observed with SOG on silicon. More precisely, this length scale corresponds to the crack replicating distance W_1 in the case of spirals and crescent alleys, and to the width W_2 of isolated bands (see inset images in Fig. 2). We extend these data with measurements extracted from the literature and with additional experiments conducted with macroscopic layers of varnish. As a striking result, the scale of the patterns is proportional to the thickness of the film h over 4 orders of magnitude. We indeed obtain $W_1 \simeq 32h$ and $W_2 \simeq 25h$, which is large in comparison with the interaction length of the usual channel cracks (on the order of h). The robustness of these patterns observed with very different types of coatings and deposition methods, such as sol-gel [13–16], magneton sputtering [18], or evaporation [17] suggests that their characteristic width is independent from both loading conditions or material properties and only depends on the thickness of the film. This robust size selection clearly indicates that these patterns are different from other spiral or oscillating fracture paths observed in systems involving thermal gradients [21], drying fronts [22], or tearing with a blunt object [23].

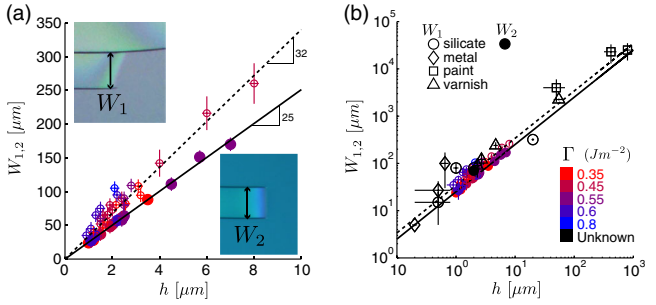

FIG. 2 (color online). (a) Width of the delaminating front in SOG films with different adhesion energies Γ_0 (color coded) as a function of the thickness h of the film for different morphologies: pitch of the spiral or wavelength of the crescent alleys (W_1, open symbols) and width of paired cracks (W_2, filled symbols). Lines correspond to linear fits of the data. (b) Generalization to a wider range of systems including data from the literature (other silicate films [13–15,20], metal films [17–19]) and macroscopic measurements on varnish or paint.

Our experimental system also allows for live observation of the quasistatic crack dynamics using a reflection microscope. Interferences fringes show that the film simultaneously delaminates as the crack propagates. Field emission gun-SEM imaging shows that the fracture fully extends to the bottom of the debonding layer (see the Supplemental Material [12]). The film may eventually readhere to the substrate far from the crack front. Delamination is thus not always obvious in postmortem images of the cracked coating, although it actually takes place during propagation (as confirmed by AFM images [12]).

Before describing these peculiar cracks, we first recall the case of classical channel cracks propagating through a thin film under an isotropic tensile stress σ. Following Griffith classical criterion, fracture propagates if the elastic energy released per unit length overcomes the fracture energy,

$$2\gamma he \geq G_c h, \quad \text{with} \quad e = h\sigma^2(1-\nu)/E, \tag{1}$$

where e is the elastic energy in the film per unit surface (h, E, and ν are, respectively, the thickness, Young modulus, and Poisson ratio of the film), and G_c is the fracture energy per unit area. The coefficient γ depends on the mismatch in elastic properties between the film and the substrate and is of order 1 for the relevant case of comparable rigidities [7]. In physical terms, γh gives the lateral size over which fracture allows stresses to relax in the bonded coating. Equation (1) shows that classical channel cracks are expected to propagate above a critical thickness $h_c = G_c E/2\gamma\sigma^2(1-\nu)$. Surprisingly, the nonstandard crack patterns displayed in Fig. 1 are observed below h_c, confirming a different fracture mechanism. In fact, fracture and delamination collaborate here, releasing residual stresses in the large delaminated area surrounded by free boundaries.

We now present a simple theoretical framework for this new collaborative mode, which explains the robustness of the fracture path geometries, and provide a general diagram for its domain of existence. We first focus on the simpler case of an isolated band, i.e., a pair of cracks propagating simultaneously [Fig. 1(f)] and then describe path-following cracks [Figs. 1(b)–1(e)].

We consider a pair of cracks propagating in a local direction θ along a symmetric, but arbitrary, path with curvilinear length s [Fig. 3(a)]. In addition to the energy released along the edges $2\gamma ehs$, which would drive the propagation of isolated channel cracks [Eq. (1)], debonding an area A is expected to completely release the residual energy eA, except in the vicinity of the debonding front where boundary conditions maintain strains parallel to the front. This incomplete release extends in an area

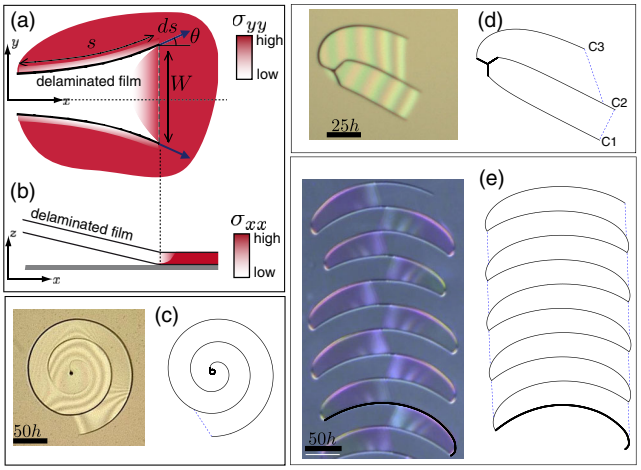

FIG. 3 (color online). (a) Delaminated symmetric band with imperfect release of stress σ_{yy} close to the debonding front. (b) The spontaneous tilt of the band releases stresses σ_{xx} ahead of the debonded zone. (c)–(e) Comparison of experimental crack paths with the prediction from energy minimization with ($\alpha = 0.0251$, $\beta = 1.26$) starting from an initial crack represented by a thick black line. The debonding front is drawn in dashed blue line.

proportional to W^2 leaving a residual energy $\alpha e W^2$ [Fig. 3(a)]. Nevertheless, the delaminated film is also free to tilt up along the debonding front, releasing stresses perpendicular to the delamination front [Fig. 3(b)]. This effects extends on a distance of order h ahead of the front, corresponding to an additional energy release $\beta e h W$. Summing the different terms finally gives the released energy

$$\mathcal{E}_r = e(A - \alpha W^2 + \beta h W + 2\gamma h s), \tag{2}$$

where α, β, γ are nondimensional constants. This expression is in agreement with experimental measurement of the strain fields obtained from image correlation and with finite element calculations conducted on a parallel band cut from a prestrained film adhering to a substrate (see the Supplemental Material [12]).

Following Griffith's criterion, symmetric cracks should propagate by ds along a given direction θ when adhesion and fracture energies, $(\Gamma W \cos\theta + 2G_c h)ds$, are balanced by the released elastic energy $d\mathcal{E}_r$, i.e., for

$$\begin{aligned} &e[W\cos\theta + 2\gamma h - 2(2\alpha W - \beta h)\sin\theta] \\ &\quad = \Gamma W \cos\theta + 2G_c h, \end{aligned} \tag{3}$$

where we have used the geometrical relations $dA = W ds \cos\theta$ and $dW = 2ds\sin\theta$. In addition, cracks are expected to propagate in the direction that maximizes the energy release rate [7,24],

$$eW\sin\theta + 2e(2\alpha W - \beta h)\cos\theta = \Gamma W \sin\theta. \tag{4}$$

Combining Eqs. (3) and (4) finally leads to

$$\sin\theta = -\frac{e}{G_c - \gamma e}(2\alpha W/h - \beta), \tag{5}$$

which predicts that the propagation is straight ($\theta = 0$) for a specific intercrack distance

$$W_2 = \frac{\beta}{2\alpha} h. \tag{6}$$

The sign of θ in Eq. (5) tends to compensate any deviation from W_2 and leads to a stable mode of propagation for self-peeling bands with constant width. In physical terms, this width optimizes the energy released [Eq. (2)], by balancing the surface energy (α term) which penalizes large W, with the line energy (β term) dominant at small W. Because the optimal width is set by elasticity alone, it is independent from the magnitude of loading, adhesion, or fracture energies, as observed in experiments (Fig. 2). A numerical estimate of the parameters α and β, and the study of stress intensity factors, provide a predicted width $W_2 = 23.7h$ in quantitative agreement with experiments (see the Supplemental Material [12]).

Although the geometry of the bands is similar for all systems, the condition for propagation does depend on the magnitude of adhesion. Indeed, the propagation of a strip is energetically possible [Eq. (3)] if the adhesion energy is exactly $\Gamma = \Gamma_2$, with

$$\frac{\Gamma_2}{e} = 1\text{–}2\left(\frac{G_c}{e} - \gamma\right)\frac{h}{W_2}. \tag{7}$$

Experimental measurements of the adhesion energy show that Γ depends on the speed of propagation (see the Supplemental Material [12]). Starting from a minimum equilibrium value Γ_0, the adhesion energy Γ is found to increase with the velocity of the front, as observed in similar systems where water activated delamination is limited by diffusion kinetics [25]. As a consequence, the propagation of a pair of parallel cracks is only possible if $\Gamma_2 > \Gamma_0$, and $\Gamma(v) = \Gamma_2$ prescribes the propagation speed v, which typically ranges from 1 to 50 μm/s in our experiments. Note that although G_c is also expected to depend on v, we did not include this effect which only changes the numerical value of the selected velocity.

We extend previous arguments to the case of crescent alleys or spirals, where a single crack follows an older fracture path of arbitrary geometry, assuming the same expression for the energy released. We derive the inclination of the debonding front (assumed straight), and obtain general analytical equations for the crack trajectory and the conditions for propagation (see the Supplemental Material [12]). The resolution of these equations provide an excellent prediction of the experimental path [see Figs. 3(c), 3(d), 3(e)]. Some particular analytical solutions

are worth mentioning. In the case of a crack interacting with a previous straight cut, we obtain a stable width,

$$W_1 = \frac{\beta h}{2\alpha}\left(\frac{1}{\sqrt{2}} + \frac{G_c/e - \gamma}{2\beta}\right), \tag{8}$$

corresponding to a debonding front tilted by an angle of 45° This relation explains the robust tendency to replicate a crack path at a well-defined distance observed in experiments [Fig. 3(c)], although the quantitative dependence of W_1 with G_c/e is difficult to capture [Fig. 2(a)]. The propagation velocity is now set by $\Gamma(v) = \Gamma_1$, with

$$\frac{\Gamma_1}{e} = 1 - \left(\frac{G_c}{e} - \gamma\right)\frac{h}{W_1}. \tag{9}$$

In the case of a crack rotating around a point (or around the tip of a straight segment), we obtain a circle of radius equal to the width W_2 of the symmetric band. Crack velocities are also identical, given by $\Gamma(v) = \Gamma_2$. Since in our system $\Gamma_2 < \Gamma_1$, cracks rotating around a tip, or paired parallel cracks, propagate at lower velocities than cracks following a straight cut. A crack following a parallel band thus catches up with the paired cracks as illustrated in Fig. 3(d) (see also movie S4 in the Supplemental Material [12]). More importantly, in the case where adhesion energy is high enough ($\Gamma_0 > \Gamma_2$), rotation around a sharp turning point (such as the extreme point of the crescent path) is not energetically possible, and the front stops. In experiments, we observe that a secondary delamination front then slowly develops and triggers the propagation of the returning branch, leading to a crescent alley [Fig. 3(e) and movie S2 in the Supplemental Material [12]].

Three main physical ingredients dictate the different crack patterns: the residual energy density per unit surface e, the fracture energy of the film G_c, and the adhesion energy for vanishing speed Γ_0. In our experiments with silicate coatings, e and Γ_0 could be varied independently by, respectively, adjusting the thickness of the film and the chemical treatment of the substrate, while G_c was set by the system. In Fig. 4, we present the morphologies of the cracks structures as a function of the two nondimensional parameters, $\gamma e/G_c$ and e/Γ_0.

In the classical picture, isolated channel cracks propagate when $\gamma e/G_c \geq 1/2$. Delamination is energetically favorable when the residual elastic energy overcomes adhesion energy, $e \geq \Gamma_0$, but this mode of failure requires free boundaries to propagate and the damaged zone is usually confined within limited regions along defects or between channel cracks. The boundaries corresponding to these classical conditions are drawn as straight lines in Fig. 4, and the pink colored domain is therefore expected to be stable. However, the collaborative mechanism occurs within this region usually recognized as safe. Two additional limiting boundaries are introduced to describe these modes: $\Gamma_0 = \Gamma_2$ which sets the condition to obtain parallel paired cracks (brown line), and $\Gamma_0 = \Gamma_1$ for follower cracks (black line). These conditions are compatible with our experiments (circles and squares represent the patterns experimentally observed) although experimental uncertainties do not allow quantitative determination of the boundaries. Crescent and paired cracks are also observed in the domain where isolated cracks are possible. Different states can indeed coexist for the same set of parameters depending on nucleation. While spirals are triggered by localized defects, crescent alleys require relatively long initial cracks to develop and parallel bands are found along rough boundaries. More complicated interacting structures can also be observed when the density of defects is increased [Fig 1(a)]. Nevertheless, we do not expect any fracture when $\Gamma_0 > \Gamma_1$, which defines a new, reduced domain for the stability of coatings (in darker pink in Fig. 4). Systems where residual stresses increase progressively (for instance, as drying takes place) follow a straight line in this diagram starting from the origin. The first failure mode encountered is therefore either classical isolated cracks or the collaborative modes if $\Gamma_0/G_c < \gamma$. This condition quantifies the fact that when adhesion energy is weaker than fracture energy, delamination collaborates with transverse fracture into a cooperative failure mode.

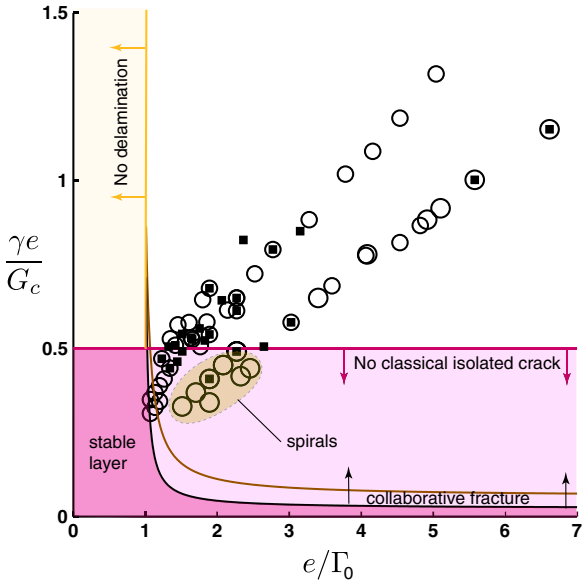

FIG. 4 (color online). Experimental observations of patterns in the $(\gamma e/G_c, e/\Gamma_0)$ plane: cracks following a previous cut (open circle, spiral or crescent) and paired cracks leading to self peeling strip (solid square). Two borders $\gamma e/G_c \geq 0.5$ (pink line) and $e/\Gamma_0 \geq 1$ (yellow line) classically define the regions where isolated channel cracks and delamination are, respectively, impossible. However, collaborative delamination cracks are observed within the light pink domain. The different patterns are observed for $\Gamma_2 > \Gamma_0$ (paired cracks above the brown curve), $\Gamma_1 > \Gamma_0$ (spirals and oscillating crescents above the black limit). Different patterns are observed for the same range of physical parameters, depending on nucleation geometries. We observe crescent patterns with larger amplitude closer to the black limit.

Although cracks are usually viewed as a failure, the extreme robustness of the self-replicated patterns induced by the collaborative mode presented here can turn fracture into a design tool. The patterns form spontaneously along a path determined completely by the geometry of the initiation spot independently from inhomogeneities of adhesion properties (often difficult to control perfectly). Recently developed micropatterning techniques allow the control of the geometry of initiation [26]. Our study provides the operating conditions for these robust patterns through a physical description of the phenomenon supported by numerical and experimental tests.

We thank ECOS C12E07, CNRS-CONICYT, and Fondecyt Grant No. N1100537 for partially funding the project. We are very grateful to Mélanie Lebental for introducing us to such beautiful crack samples.

*Joel.Marthelot@espci.fr

[1] G. Gioia and M. Ortiz, Adv. Appl. Mech. **33**, 119 (1997).
[2] N. Padture, M. Gell, and E. Jordan, Science **296**, 280 (2002).
[3] J. Haldar, D. An, L. Alvarez de Cienfuegos, J. Chen, and A. Klibanov, Proc. Natl. Acad. Sci. U.S.A. **103**, 17667 (2006).
[4] J. A. Rogers, T. Someya, and Y. Huang, Science **327**, 1603 (2010).
[5] N. Bowden, S. Brittain, A. G. Evans, J. W. Hutchinson, and G. M. Whitesides, Nature (London) **393**, 146 (1998).
[6] D. Vella, J. Bico, A. Boudaoud, B. Roman, and P. Reis, Proc. Natl. Acad. Sci. U.S.A. **106**, 10901 (2009).
[7] J. Hutchinson and Z. Suo, Adv. Appl. Mech. **29**, 63 (1992).
[8] A. Atkinson and R. Guppy, J. Mater. Sci. **26**, 3869 (1991).
[9] K. A. Shorlin, J. R. de Bruyn, M. Graham, and S. W. Morris, Phys. Rev. E **61**, 6950 (2000).
[10] S. Bohn, S. Douady, and Y. Couder, Phys. Rev. Lett. **94**, 054503 (2005).
[11] V. Lazarus and L. Pauchard, Soft Matter **7**, 2552 (2011).
[12] See the Supplemental Material http://link.aps.org/supplemental/10.1103/PhysRevLett.113.085502 for movie sequences of the experiments, details on material properties, calculations of stress fields, and a model for following cracks.
[13] M. Lebental, Ph.D. thesis, École Normale Supérieure de Cachan, 2007.
[14] M. Sendova and K. Willis, Appl. Phys. A **76**, 957 (2003).
[15] N. Wan, J. Xu, T. Lin, L. Xu, and K. Chen, Phys. Rev. B **80**, 014121 (2009).
[16] D. Wu, Y. Yin, H. Xie, and F. Dai, Chin. Phys. Lett. **30**, 036801 (2013).
[17] B. Bozzini, M. Boniardi, A. Gianoncelli, B. Kaulich, C. Mele, M. Prasciolu, G. Scarselli, and M. Kiskinova, in *Proceedings of Crack Paths (CP2012), Gaeta, Italy, 2012*, p. 595, http://www.gruppofrattura.it/pdf/cp/CP2012.
[18] D. Meyer, T. Leisegang, A. Levin, P. Paufler, and A. Volinsky, Appl. Phys. A **78**, 303 (2004).
[19] V. Bursíková, P. Sládek, P. Stáhel, and J. Bursík, J. Non-Cryst. Solids **352**, 1238 (2006).
[20] J. Malzbender and G. de With, Thin Solid Films **359**, 210 (2000).
[21] A. Yuse and M. Sano, Nature (London) **362**, 329 (1993).
[22] K.-T. Leung, L. Józsa, M. Ravasz, and Z. Néda, Nature (London) **410**, 166 (2001).
[23] B. Audoly, P. M. Reis, and B. Roman, Phys. Rev. Lett. **95**, 025502 (2005).
[24] B. Cotterell and J. Rice, Int. J. Fract. **16**, 155 (1980).
[25] Y. Lin, T. Tsui, and J. Vlassak, Acta Mater. **55**, 2455 (2007).
[26] K. Nam, I. Park, and S. Ko, Nature (London) **485**, 221 (2012).